Imaging magnonic frequency multiplication in nanostructured antidot lattices

Felix Groß,[1,*] Markus Weigand,[2] Ajay Gangwar,[3] Matthias Werner,[1] Gisela Schütz,[1] Eberhard J. Goering,[1] Christian H. Back,[4] and Joachim Gräfe[1,†]

[1]*Max Planck Institute for Intelligent Systems, 70569 Stuttgart, Germany*
[2]*Helmholtz-Zentrum Berlin für Materialien und Energie, 12489 Berlin, Germany*
[3]*Department of Physics, University of Regensburg, 93053 Regensburg, Germany*
[4]*Technical University Munich, 85748 Garching, Germany*

(Received 14 April 2022; revised 17 June 2022; accepted 19 July 2022; published 29 July 2022)

Frequency multiplication is an essential part of electronics and optics which led to numerous indispensable applications. In this paper, we utilize a combination of scanning transmission x-ray microscopy and micromagnetic simulations to directly image magnonic frequency multiplication by means of dynamic real-space magnetization measurements. We experimentally demonstrate frequency multiplication up to the seventh order, which enables the generation of nanoscale spin waves at 6 GHz with excitation frequencies of less than 1 GHz. Good agreement between the experiment and micromagnetic simulations allows us to build a micromagnetic model capable of predicting conversion efficiencies and multiplexing capabilities of the system. Furthermore, simulations reveal that more than two rows of antidots do not increase the conversion efficiency substantially. By enabling magnonic multiplexing with low input frequencies while not exceeding the size of a few microns, the device will lead to numerous applications, further advancing the capabilities of magnonic data transmission.

DOI: 10.1103/PhysRevB.106.014426

I. INTRODUCTION

Frequency multiplication is a well-known nonlinear phenomenon widely applied in electronics [1–6] and optics [7–12] as well as spintronics [13–19]. Although the output efficiency depends on the frequency, the chosen approach, and additional technological limitations, frequency multiplication has proven to be a powerful approach for the generation of high-frequency electromagnetic radiation for a wide range of applications.

The precession of magnetic moments around their equilibrium point can be described by bosonic quasiparticles known as magnons or spin waves. Magnons [20–22] are inherently tied to nonlinear effects due to the nonlinear dynamics of the underlying Landau-Lifshitz-Gilbert equation [23,24]. This manifests in effects such as spontaneous second-harmonic generation [14], general frequency doubling or tripling [15–17], and many-magnon scattering [25–31]. Although nonlinear magnonic effects are complex and difficult to utilize, some of the most promising magnonic devices for applications critically depend on them [32,33].

What makes frequency multiplying of spin waves particularly interesting is the fact that the direct excitation with a microstrip antenna [34,35] is accompanied by wavelength limits determined by the applied frequency and the spatial features of the sample, and therefore, the spatial resolution of the structuring process [36–49]. However, if the magnetic structure itself generates higher harmonic frequencies, the limits given by sample fabrication and excitation frequency are softened. First steps in this direction have already been taken [14] by demonstrating that magnonic frequency multiplication allows excitation of types of spin waves that would otherwise not exist in the system, even when driven at multiples of the input frequency.

It has been proposed that a wide range of magnetic textures are able to take advantage of nonlinear processes by acting as frequency multipliers [19]. This method allows frequency multiplication to be performed over a large range of input frequencies and powers. However, the effect is based on eigenfrequencies of the corresponding quasiparticle and therefore does not allow arbitrary frequencies. Very recent experimental work has shown that the generation of harmonics up to the 60th order is possible when depositing magnetic thin films on top of a coplanar waveguide [50], however, only for low external bias fields of up to 2 mT. Thereby, the authors were able to excite spin waves with wavelengths in the single micron range with frequencies of only a few hundred MHz.

In this paper, we use higher harmonic generation to create spin waves in nanostructured antidot lattice thin films. With excitation frequencies of less than 1 GHz we are able to excite spin waves of 300 nm wavelength being arguably close to the exchange threshold. By means of time-resolved scanning transmission x-ray microscopy (TR-STXM), we can directly image magnetization dynamics in real space and

*fgross@is.mpg.de
†graefe@is.mpg.de

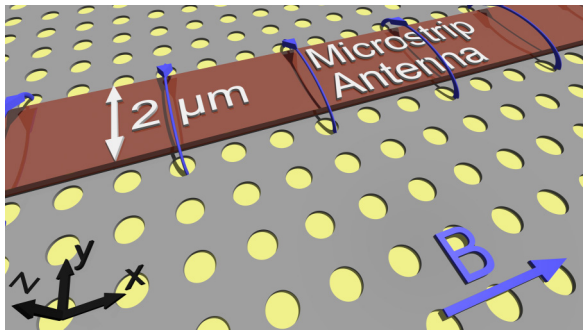

FIG. 1. Sketch of the 50 nm permalloy (gray) antidot sample deposited on an x-ray transparent Si_3N_4 membrane (yellow). Spin waves are excited by an rf current in a 2-μm-wide microstrip antenna. An external field is applied parallel to the antenna to saturate the sample.

time domain. Complementing our findings with simulations allows us to discuss the order-dependent spin-wave amplitude for which we find frequency-dependent excitation thresholds. Varying the geometry in simulations, we find that the frequency multiplication efficiency which critically depends on the magnetic structure. Nevertheless, structures as small as a few micrometers in diameter already lead to very high conversion efficiencies for higher harmonics.

II. METHODS

STXM measurements were performed on a 50-nm-thick $Fe_{20}Ni_{80}$ (permalloy/Py) thin film, deposited by magnetron sputtering at a base pressure lower than 5×10^{-9} mbar. For oxidation protection, additional 5 nm Al were added on top of the Py in the same sputtering process. As an x-ray transparent substrate, a Si_3N_4 membrane sample chip was used. To generate a highly inhomogeneous magnetic film, necessary for higher harmonic generation, antidots with a hole diameter $d = 450$ nm and a center to center distance $a = 900$ nm were structured over the entire thin film area by electron beam lithography. A more detailed STXM picture of the antidots can be found elsewhere [51]. To electrically insulate the antenna from the magnetic film, additional 10 nm of Al_2O_3 were added via atomic layer deposition. For spin wave excitation, a 2-μm-wide radio frequency (rf) microstrip antenna consisting of Cr(10 nm)/Cu(150 nm)/Al(5 nm) was structured on top of the magnetic film via a combination of optical and electron beam lithography and deposited using physical vapor deposition. The sample geometry is illustrated in Fig. 1.

Micromagnetic simulations were performed using the MUMAX^3 simulation package [52]. As in the experiment, spin waves were excited by a locally oscillating magnetic field applied perpendicular to the static external field. The damping coefficient was set to $\alpha = 6.7 \times 10^{-3}$, while the exchange constant and the saturation magnetization were fixed at $A_{ex} = 13 \times 10^{-12}$ J/m and $M_s = 6 \times 10^5$ A/m, respectively. The values were chosen to match simulations and experimental results qualitatively. Although the saturation magnetization is quite low for permalloy (in bulk usually 6.4×10^5 A/m), we previously found good agreement for theoretical and experimental results using a reduced magnetization [36,53,54]. The simulations were performed with a cell size of approximately 7 nm × 7 nm × 25 nm and a fixed time step of 0.15 ps. To simulate a continuous thin film, periodic boundary conditions were used.

TR-STXM experiments were conducted at the BESSY II synchrotron radiation facility. The MAXYMUS end station at the UE46-PGM2 beamline allows for high-temporal as well as spatial resolutions down to 50 ps and 20 nm. Four rotatable permanent magnets allow for the generation of an external magnetic field of up to 240 mT [55]. Samples were illuminated under perpendicular incidence of circularly polarized x-ray light, whose energy was set to the maximum of the Fe L_3 edge to achieve optimal x-ray magnetic circular dichroism (XMCD) contrast for imaging [56]. A double lock-in technique allows for time-resolved XMCD contrast at any arbitrary rf frequency and the pixelwise acquisition of spin-wave movies in real space and time domain. A fast Fourier transformation (FFT) is utilized for frequency filtering and analysis in reciprocal as well as frequency space. For additional information on spin-wave measurements and evaluation with TR-STXM, the reader is referred elsewhere [36,48,51,53,54,57–62].

III. RESULTS AND DISCUSSION

A. Imaging magnonic frequency multiplication

To experimentally investigate higher spin wave harmonics, we utilized an antidot sample and evaluated its frequency multiplier capabilities. A schematic of the sample can be seen in Fig. 1. Spin waves were excited with a continuous rf excitation at a base frequency of $f_{base} = 0.93$ GHz and an external field of $B_{ext} = 20$ mT. All frequency components presented throughout the paper are obtained from a temporal FFT of the dynamic magnetization to the 0.93 GHz excitation and therefore display the response of spin waves at higher harmonic frequencies.

A real-space illustration of the magnetization dynamics obtained from STXM is displayed in Figs. 2(a)–2(f). The spin-wave amplitude is encoded in color saturation while the phase is displayed as hue. The position of the microstrip antenna is indicated by a white overlay.

The frequency response of the system at higher harmonics is very different to the response at $f_{base} = 0.93$ GHz. While the base frequency in Fig. 2(a) mainly excites the channel mode plus some oscillations near the antidot edges, it changes to a pattern with multiple nodes across the channel for higher frequencies, as marked by the arrows in Fig. 2(e). Although the signal-to-noise ratio decreases with higher harmonics, a signal can be picked up for frequencies of up to 5.61 GHz, corresponding to a sixfold increase in frequency.

Figures 2(g)–2(l) displays simulations of the system at the same excitation frequency of $f_{base} = 0.93$ GHz, however, at a magnetic field of $B_{ext} = 30$ mT. This discrepancy is caused by the calibration of the external magnetic field in the experiment, which is generated by four rotatable permanent magnets [51]. Nevertheless, the simulations fit the experiments well, which allows us to obtain a more thorough understanding of the system by utilizing the micromagnetic model.

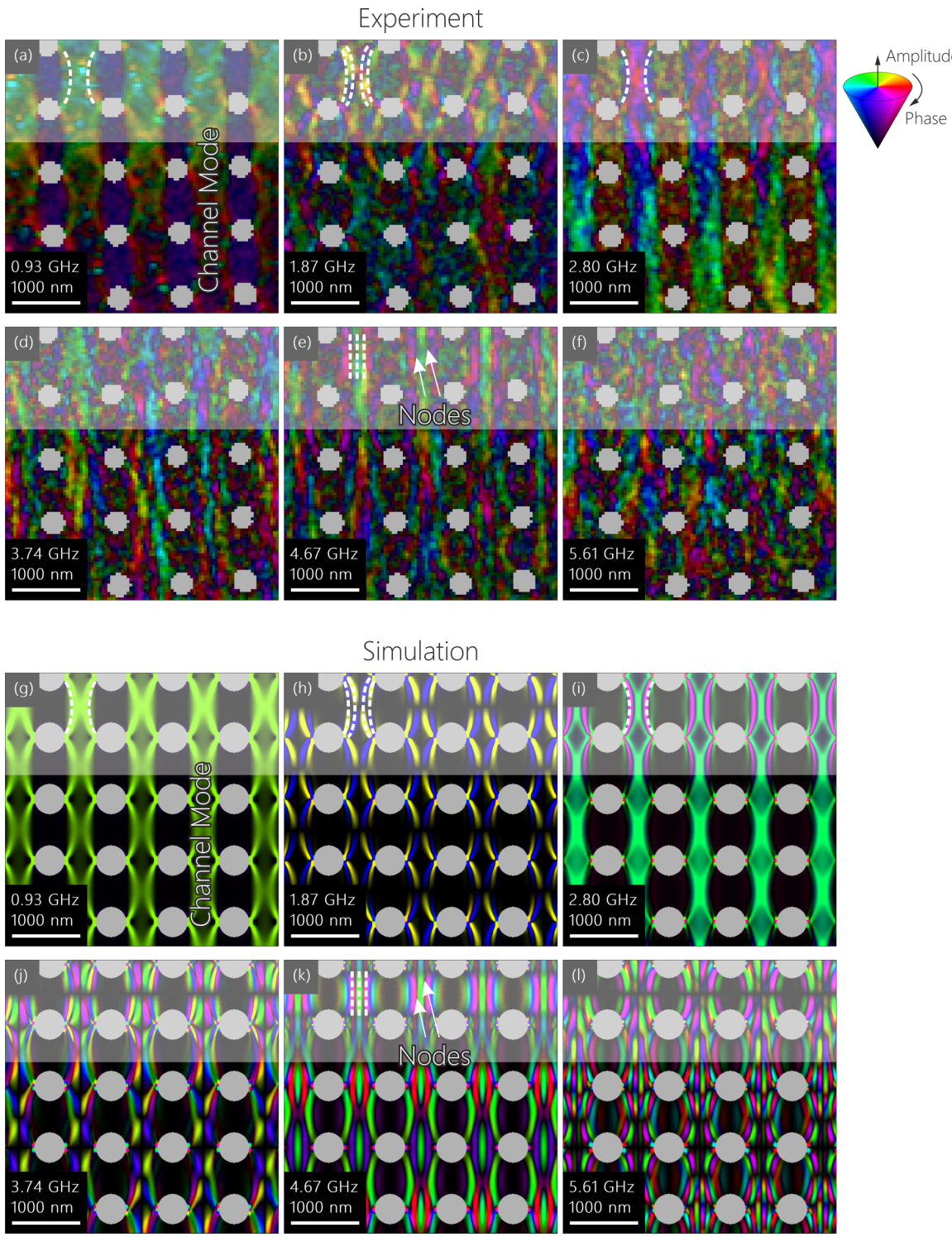

FIG. 2. Comparison of the experimentally measured and simulated magnetization dynamics at a base excitation frequency of 0.93 GHz. Spin-wave amplitude is encoded in color saturation while the phase is displayed as hue. The position of the microstrip antenna is indicated by a light white overlay: (a)–(f) Results obtained from a temporal FFT of the experimental data. Higher harmonics of the base frequency displayed in (a) are illustrated in (b)–(f). (g)–(l) Simulated results with the same base excitation frequency again obtained from a temporal FFT. White lines and annotations highlight the similarities between the experiment and the simulation, such as standing wave patterns and the general shape of the spin waves.

The simulated base frequency response is displayed in Fig. 2(g) while the higher harmonics are displayed in Figs. 2(h)–2(l). As displayed in the comparison between simulation and experiment, the simulation resembles the results measured in the experiment reasonably well. The base frequency excites spin waves mainly traveling down the channel whereas higher frequencies start to excite transversal standing spin waves between the individual antidots. The similarity is

indicated by dashed white lines and valid up to high frequencies [cf. Figs. 2(e) and 2(k)] for which the same red-green-red pattern can be observed in the experiment as well as the simulations. In the experiment, as well as in the simulations, it is visible that due to the influence of the antenna, the spin-wave amplitude (color saturation) is highest directly underneath it. For frequencies above 5 GHz, the signal-to-noise ratio in the experiment decreases due to the temporal resolution provided by the synchrotron.

To show that frequency multiplication is not restricted just to 0.93 GHz, the Supplemental Material [63] also includes experimental examples for base frequencies of 1.41 GHz and 1.87 GHz. Additionally, by comparing Fig. 2(b) and Fig. Sup. 1(g) from the Supplemental Material, it is visible that although oscillating at the same frequency (1.87 GHz), the spin wave excited by frequency multiplication can look very different from a spin wave excited directly. Similar effects have been observed previously [14]. Therefore, we conclude that the excited higher harmonic modes do not correspond to the conventional eigenmodes of the system. Hence, using frequency multiplication, additional modes can be excited within the antidot lattice which would otherwise not exist in the system.

While the generation of short spin waves is usually accompanied by some kind of rf excitation at high frequencies, the presented results display the possibility to instead exploit the nonlinearity of the underlying differential equation. Usually, spin waves excited at around 1 GHz exhibit wavelengths in the micron range. However, analyzing Fig. 2(e) in Fourier space reveals that frequency multiplication allows us to generate spin waves with wavelengths of approximately 300 nm at just 0.93 GHz.

The generation of higher harmonic spin-wave modes can be qualitatively understood by analyzing the projection of the magnetization vector along each component, assuming its magnitude equals the saturation magnetization M_S [14,17,64]:

$$M_x^2 + M_y^2 + M_z^2 = M_S^2. \tag{1}$$

Assuming an external magnetic field along the x axis, for an elliptical precession of frequency ω and magnitudes m_y and m_z along the y axis and z axis, respectively, the projection of M along the x direction has the general form of

$$M_x^2 = M_S^2 - \tfrac{1}{2}\left[\left(m_y^2 - m_z^2\right)\cos(2\omega t) + m_z^2 + m_y^2\right]. \tag{2}$$

In the case of elliptical precessions, where $m_y^2 - m_z^2 \neq 0$, the M_x component oscillates with twice the excitation frequency. For a circular precession with $m_y = m_z = m_{yz}$, the equation can be simplified to

$$M_x^2 = M_S^2 - m_{yz}^2, \tag{3}$$

which compared to Eq. (2) does not have a time dependency anymore. For magnetic thin films, the difference of in-plane and out-of-plane anisotropy causes the spins to perform elliptical instead of circular precession [16], which in turn allows for multiples of the base frequency to occur. However, not every thin film experiences frequency multiplication as efficient as presented here. In addition to the elliptical precession, the antidots generate a highly inhomogeneous magnetization. Due to the tilt of the magnetization at the edges of each antidot [51], the time-dependent oscillation in Eq. (2) now has components which are not parallel to the magnetization, therefore exerting a torque and rendering the excitation of higher harmonics much more efficient.

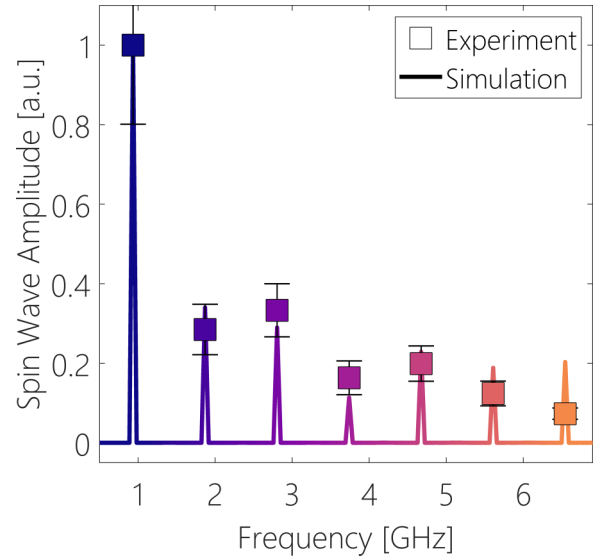

FIG. 3. Experimental and simulated frequency multiplication (spin wave amplitude over frequency) for a base frequency of $f_{\text{base}} = 0.93$ GHz: Experimental results are displayed as scatter plot, simulated results as line plot. The values for the base frequency are normalized to 1 for the experimental and the simulated data set. For high frequencies, the experimental spin-wave amplitude is reduced due to the temporal limitation of the synchrotron setup. Error bars are estimated by subtracting a slightly smoothed version of the amplitude from its original counterpart, resulting in a noise residuum. The residuum is subsequently used to estimate the noise floor of the measurement. The color code denotes the frequency and will be used throughout the paper.

While the presented images of the magnetization dynamics provide an illustrative possibility to qualitatively compare experimental and simulated results, a quantitative comparison in the frequency domain is needed to determine the efficiency of the frequency multiplication. We evaluated the mean spin-wave amplitude of simulated and experimental results for frequencies of up to 6.54 GHz and normalized both data sets with respect to the base frequency $f_{\text{base}} = 0.93$ GHz.

A comparison between experimental and simulated results is displayed in Fig. 3. As displayed, the system converts some of its energy to higher harmonics ($2f_{\text{base}}, 3f_{\text{base}}, 4f_{\text{base}}, \ldots$), while the simulations show that the amplitude almost vanishes between multiples of the base frequency. The relative values of each frequency can be regarded as the conversion efficiency belonging to a certain harmonic. No energy being dissipated to intermediate frequencies renders the frequency multiplication much more efficient, and therefore also extremely effective for high frequencies.

Experimental and simulated results are in good agreement up to frequencies of about 5 GHz, which is when the experimental spin-wave amplitude starts to decrease. This is caused by the same restrictions that also lower the signal-to-noise ratio in Fig. 2(f). The synchrotron's temporal resolution, given by the electron bunch length and stability, is not sufficient anymore to fully resolve the spin wave frequency, causing

the observed spin wave amplitude to be reduced at high frequencies.

It can be seen that some frequencies ($2f_{\text{base}} = 1.87\,\text{GHz}$) are less populated than the subsequent harmonic ($3f_{\text{base}} = 2.80\,\text{GHz}$), which is visible in the experiment as well as in the simulation and can also be observed in real space in Figs. 2(b), 2(c), 2(h), and 2(i). This behavior can be explained by the shape of the spin wave, which can either oscillate over the entire width of the channel [Figs. 2(c) and 2(i)] or form nodes [Figs. 2(b) and 2(h)]. This results in an overall lower average amplitude, but provides higher amplitudes at the actual oscillation points. Overall, we observe conversion rates of 12.4%–33.3%) for frequencies up to 6.54 GHz in the experiment. These rates are in good agreement with previously reported conversion efficiencies for higher harmonics in permalloy [50].

B. Excitation field dependency

Frequency multiplication and nonlinear effects, in general, critically depend on the amount of driving power provided to the system. Raising the driving power increases the spin precession angle, and hence increases the deviation of the differential equation from its linear approximation. We therefore investigated the dependency of higher harmonic amplitudes on the oscillating excitation field applied in the simulation. This dependency is depicted in Fig. 4(a). Since the system only shows a magnonic response at the base frequency and at higher harmonics anyway, the frequencies with amplitudes close to zero are omitted in this illustration and only multiples of the base frequency are plotted.

From the partially linear slope of each curve in a double logarithmic plot, we can conclude that the spin-wave amplitude A follows a power law of the form

$$A \sim B_{\text{max}}^{I}, \tag{4}$$

within *regime 1* and *regime 2*, where B_{max} and I corresponds to the amplitude of the excitation field and the growth exponent, respectively.

As can be seen in Fig. 4(a), all higher harmonics experience low spin-wave amplitudes at low excitation fields. However, lower harmonics have a lower excitation threshold, which needs to be overcome before the amplitude starts rising. To quantify this, we used a constant fit for the baseline amplitude and a linear fit for the initial slope of the curve as indicated by the horizontal dashed line and the line labeled as *regime 1*. The excitation field at which the two lines cross is a measure for the excitation threshold. The excitation threshold as function of harmonic frequency can be seen in Fig. 4(b). The initial data point is omitted since there is no excitation threshold for the base frequency which excited magnons over the entire excitation range. As displayed, the excitation threshold increases with increasing frequency, which shows that additional power is needed to effectively excite higher harmonics.

While the excitation threshold increases for higher harmonics, it can be seen in Fig. 4(a) that the amplitude tends to increase faster at higher frequencies. The initial growth exponent of the spin-wave amplitude can be extracted from the linear fit labeled *regime 1* in Fig. 4(a). The slope of the linear fit in a double logarithmic plot equals the magnitude of the exponent I and therefore the amplitude scaling as function of frequency. The amplitude growth exponents extracted from the fits are plotted as squares in Fig. 4(c). Expanding on previous works reporting on the growth exponent of the second [15,17] and third [15] harmonic, our findings for the

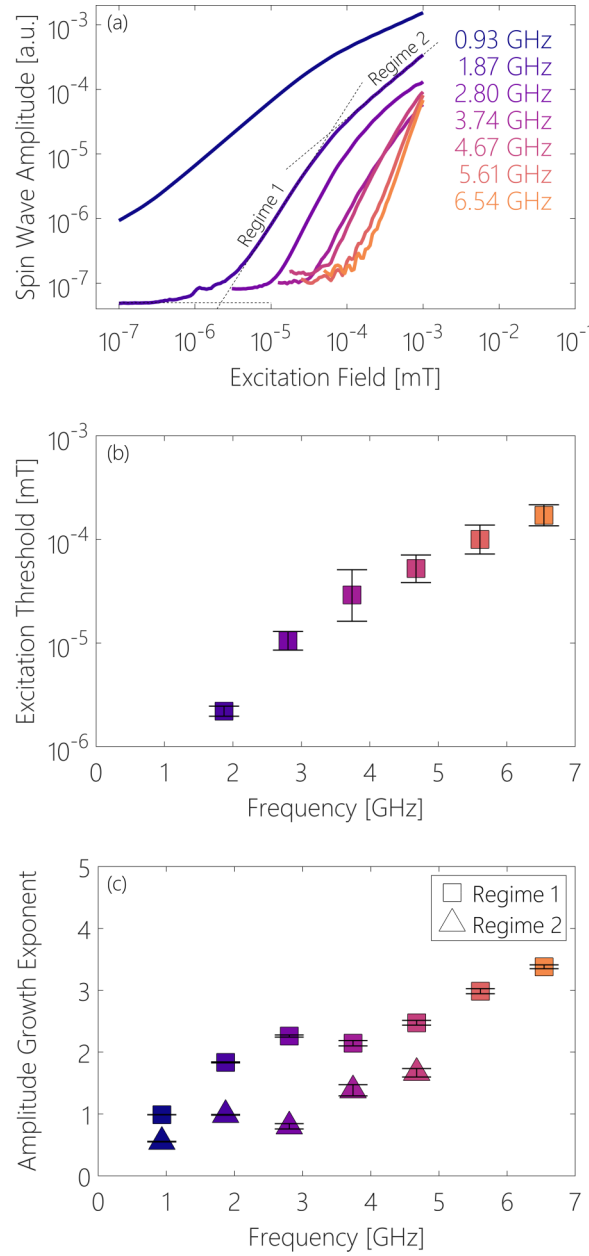

FIG. 4. Simulated excitation field dependency of the frequency multiplication at a base frequency of $f_{\text{base}} = 0.93\,\text{GHz}$. The color code indicates frequency: (a) Spin-wave amplitude as a function of excitation field for the base frequency and harmonics up to 6.54 GHz. (b) Threshold of the excitation field at which the spin-wave amplitude starts to increase. (c) Amplitude growth exponent as function of frequency, which indicates how fast the spin wave amplitude increases once the threshold is reached. The exponent is extracted from the fit indicated by the dashed line labeled as *regime 1* in Fig. 4(a). Lower harmonics have a second regime at high excitation powers. Error bars are extracted from the 95 % confidence intervals of the fits displayed in (a).

second-harmonic exponent ($I_2 = 1.83$) are in good agreement with previous experiments ($I_2 = 2$) [15]. However, other experiments also report on exponents as high as $I_2 = 2.8$ for the second harmonic [17]. We assume that the exponent critically depends on the sample geometry and the predominant frequency multiplying mechanism. While we can report an almost linear increase in amplitude for the base frequency ($I_1 = 0.99$), we also find that in this particular system the growth exponent for higher harmonics does not directly scale with the corresponding harmonic as suggested in Ref. [15], which leads to an exponent of only $I_7 = 3.38$ for the seventh harmonic. The combination of excitation threshold as well as growth exponent demonstrates that higher harmonics tend to be generated at higher excitation fields, however, their amplitude increases faster than the amplitude of lower frequencies.

Lower harmonics tend to form a second growth regime at higher excitation powers, for which the growth exponent is slightly lower than for the first regime. We assume that this second growth regime is a consequence of higher harmonics forming in the system. The higher harmonics tend to absorb more power at higher excitation fields, leading to a relative reduction of the power available to the fundamental mode and lower harmonics. The second regime is included in Fig. 4(c) and indicated by triangles. It can be seen that the sixth and seventh harmonics do not experience such a reduction in the amplitude growth exponent, further supporting the hypothesis that the amplitude loss is caused by even higher harmonics which are not as dominant after the seventh harmonic.

C. Geometry optimization

As already indicated by the results presented in Fig. 4, the conversion efficiency into spin waves of higher frequencies strongly depends on the geometry that the spin waves are excited in. The insets in Fig. 5 display the simulated geometries, which consist of an increasing number of antidot rows excited by the same rf field. The main diagram of Fig. 5 displays the spin-wave amplitude normalized with respect to the base frequency $f_{\text{base}} = 0.93\,\text{GHz}$.

It is clearly visible that the relative spin wave conversion efficiency drastically depends on the geometry used for the conversion. The system without any antidots (purple graph) does not experience any higher harmonic generation, proving that some kind of magnetic perturbation and therefore a magnetization gradient is needed for the efficient generation of higher harmonics. Hence, an unstructured continuous magnetic thin film cannot be utilized to efficiently excite higher harmonic frequencies.

However, exciting a structure consisting of just one row of antidots already drastically increases the conversion efficiency as displayed by the dark green graph. Although the conversion efficiency of the second harmonic is already at about 24.1 % for a single row of antidot lattices, it can be further increased by adding a second row, as displayed by the light green graph. While this only increases the amplitude of the second harmonic (1.87 GHz) by a factor of 1.15, the impact is more visible for harmonics above the second one. For example, the amplitude of the third (2.80 GHz) and seventh (6.54 GHz) harmonic increases by a factor of 2.4 and 3.3, respectively.

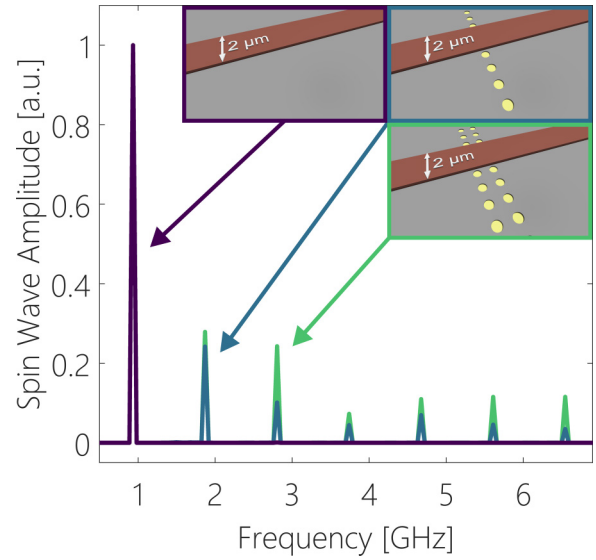

FIG. 5. Simulated conversion efficiencies of higher harmonic spin waves for three different geometries: All results are normalized with respect to the base excitation frequency of $f_{\text{base}} = 0.93\,\text{GHz}$. The three insets display the geometries of the different cases which are no antidots (purple), one row of antidots (dark green), and a double row of antidots (light green).

In the simulations, we find that adding more than two rows of antidots does not increase the conversion efficiency significantly. It turns out that using just two rows is enough to reach the full potential of the system for most of the harmonics. Adding additional rows changes the efficiency for some frequencies in the lower percentile range but the gain is nowhere near as much as when adding the first or second row. However, this has the advantage that potential implementations in thin films, where rows of antidots act as frequency multipliers, do not require much space for frequency conversion. Two rows in the range of 1 μm to 2 μm are sufficient, which leaves plenty of space for other magnonic operating elements.

IV. CONCLUSION

Frequency multiplication has proven to be a powerful tool for various technical applications in different fields of physics and engineering. In this paper, we presented experimental real-space images of magnonic frequency multiplication by utilizing nanostructured antidot lattice. The structure is able to serve as a frequency multiplier, allowing us to measure a magnonic response of the system at frequencies up to seven times the base excitation frequency. This creates opportunities for the generation of short-wavelength spin waves with low excitation frequencies, the excitation of multiple frequencies with just one base frequency for multiplexing purposes, and higher data transmission rates for spin-wave transmitters.

Scanning transmission x-ray microscopy has been utilized to experimentally verify the frequency-multiplying capabilities of the structure. By comparing experimental real-space images to micromagnetic simulations, we find reasonable agreement not only for the generated spin-wave patterns at higher harmonics but also for the quantitative spin-wave amplitudes at multiplying frequencies as high as 6.54 GHz.

The frequency multiplying capabilities allow us to excite nanoscale spin waves with approximately 300 nm wavelength at excitation frequencies as low as 0.93 GHz, measured by Fourier analysis. High conversion efficiencies between 12.4% and 33.3% in the experiment allow for efficient multiplexing capabilities. These results pave the way for nanoscaled magnonic devices operating at low and accessible input frequencies.

Moreover, the agreement of the micromagnetic model and the experiment allows us to draw additional conclusions which cannot be drawn from the experimental data alone, such as the spin-wave amplitude as a function of the excitation field strength. We find that each of the harmonic frequencies has an increasing excitation threshold, which needs to be overcome to excite the corresponding harmonic. As soon as this threshold is reached, the amplitude starts to rise with a characteristic amplitude growth exponent, which also increases with frequency. While the growth exponent of the corresponding harmonic tends to slightly decrease at higher excitation amplitudes, the growth exponent also increases for higher orders. Therefore, the amplitude of higher order harmonics only starts to rise above noise level at higher excitation fields, but increases more rapidly after that. We find growth exponents between $I_1 = 0.99$ (almost linear growth) and $I_7 = 3.38$ (exponential growth).

The micromagnetic model has also been used to predict conversion efficiencies of magnonic devices. Studying the dependency of the spin-wave amplitude on the geometric parameters of the lattice, we find that the frequency-multiplying efficiency has a complex relation to the antidot lattice parameters. While one row of antidots already allows for high efficiency, higher harmonic generation is maximized for a total of two antidot rows. Additional rows hardly increase the conversion efficiency. Thus, the system allows for maximum efficiency without exceeding the size of a few micrometers. This will prove to be useful not only for the excitation of small-wavelength spin waves with low frequencies but also as a generation source for magnonic multiplexing applications. The presented results create room for additional studies about higher harmonic spin wave generation, geometric control affecting the conversion efficiency, and magnonic data transmission by multiplexing.

ACKNOWLEDGMENTS

The authors thankfully acknowledge Maciej Krawczyk and Mateusz Zelent for fruitful discussions. The authors thank Michael Bechtel and Iuliia Bykova for support during beam times. Helmholtz Zentrum Berlin is acknowledged for allocating beam time at the BESSY II synchrotron radiation facility. Financial support by the Baden-Württemberg Stiftung in the framework of the Kompetenznetz Funktionelle Nanostrukturen is gratefully acknowledged.

[1] J. E. Carlstrom, R. L. Plambeck, and D. D. Thornton, A continuously tunable 65-15-GHz Gunn oscillator, IEEE Trans. Microwave Theory Techn. **33**, 610 (1985).

[2] N. Erickson, High efficiency submillimeter frequency multipliers, IEEE MTT-S **3**, 1301 (1990).

[3] A.V. Raisanen, Frequency multipliers for millimeter and submillimeter wavelengths, Proc. IEEE **80**, 1842 (1992).

[4] P. H. Siegel, Terahertz Technology, IEEE Trans. Microwave Theory Techn. **50**, 910 (2002).

[5] J. Ward, E. Schlecht, G. Chattopadhyay, A. Maestrini, J. Gill, F. Maiwald, H. Javadi, and I. Mehdi, Capability of THz sources based on Schottky diode frequency multiplier chains, IEEE MTT-S **3**, 1587 (2004).

[6] G. Chattopadhyay, E. Schlecht, J. S. Ward, J. J. Gill, H. H. S. Javadi, F. Maiwald, and I. Mehdi, An all-solid-state broadband frequency multiplier chain at 1500 GHz, IEEE Trans. Microwave Theory Techn. **52**, 1538 (2004).

[7] D. A. Kleinman, Theory of second harmonic generation of light, Phys. Rev. **128**, 1761 (1962).

[8] R. W. Terhune, P. D. Maker, and C. M. Savage, Optical Harmonic Generation in Calcite, Phys. Rev. Lett. **8**, 404 (1962).

[9] G. D. Boyd, A. Ashkin, J. M. Dziedzic, and D. A. Kleinman, Second-harmonic generation of light with double refraction, Phys. Rev. **137**, A1305 (1965).

[10] R. C. Miller, Optical harmonic generation in single crystal BaTiO3, Phys. Rev. **134**, A1313 (1964).

[11] D. A. Kleinman, A. Ashkin, and G. D. Boyd, Second-harmonic generation of light by focused laser beams, Phys. Rev. **145**, 338 (1966).

[12] M. V. Hobden, Phase-matched second-harmonic generation in biaxial crystals, J. Appl. Phys. **38**, 4365 (1967).

[13] M. Fiebig, T. Lottermoser, D. Fröhlich, A. V. Goltsev, and R. V. Pisarev, Observation of coupled magnetic and electric domains, Nature (London) **419**, 818 (2002).

[14] V. E. Demidov, M. P. Kostylev, K. Rott, P. Krzysteczko, G. Reiss, and S. O. Demokritov, Generation of the second harmonic by spin waves propagating in microscopic stripes, Phys. Rev. B **83**, 054408 (2011).

[15] V. E. Demidov, H. Ulrichs, S. Urazhdin, S. O. Demokritov, V. Bessonov, R. Gieniusz, and A. Maziewski, Resonant frequency multiplication in microscopic magnetic dots, Appl. Phys. Lett. **99**, 012505 (2011).

[16] T. Sebastian, T. Brächer, P. Pirro, A. A. Serga, B. Hillebrands, T. Kubota, H. Naganuma, M. Oogane, and Y. Ando, Nonlinear Emission of Spin-Wave Caustics from an Edge Mode of a Microstructured $Co_2Mn_{0.6}Fe_{0.4}Si$ Waveguide, Phys. Rev. Lett. **110**, 067201 (2013); https://www.ncbi.nlm.nih.gov/pubmed/23432296.

[17] O. Rousseau, M. Yamada, K. Miura, S. Ogawa, and Y. Otani, Propagation of nonlinearly generated harmonic spin waves in microscopic stripes, J. Appl. Phys. **115**, 053914 (2014).

[18] P. Němec, M. Fiebig, T. Kampfrath, and A. V. Kimel, Antiferromagnetic opto-spintronics, Nat. Phys. **14**, 229 (2018).

[19] D. R. Rodrigues, J. Nothhelfer, M. Mohseni, R. Knapman, P. Pirro, and K. Everschor-Sitte, Nonlinear Dynamics of Topological Ferromagnetic Textures for Frequency Multiplication, Phys. Rev. Applied **16**, 014020 (2021).

[20] V. V. Kruglyak, S. O. Demokritov, and D. Grundler, Magnonics, J. Phys. D **43**, 264001 (2010).

[21] B. Lenk, H. Ulrichs, F. Garbs, and M. Münzenberg, The building blocks of magnonics, Phys. Rep. **507**, 107 (2011).

[22] M. Krawczyk and D. Grundler, Review and prospects of magnonic crystals and devices with reprogrammable band structure, J. Phys.: Condens. Matter **26**, 123202 (2014); https://www.ncbi.nlm.nih.gov/pubmed/24599025.

[23] L. Landau and E. Lifshitz, On the theory of the dispersion of magnetic permeability in ferromagnetic bodies, in *Perspectives in Theoretical Physics*, edited by L. P. Pitaevskiĭ (Elsevier, New York, 1992), Chap. 3, p. 51.

[24] T. L. Gilbert, Classics in magnetics: A phenomenological theory of damping in ferromagnetic materials, IEEE Trans. Magn. **40**, 3443 (2004).

[25] B. Heinrich, J. F. Cochran, and R. Hasegawa, FMR linebroadening in metals due to two-magnon scattering, J. Appl. Phys. **57**, 3690 (1985).

[26] K. Lenz, H. Wende, W. Kuch, K. Baberschke, K. Nagy, and A. Jánossy, Two-magnon scattering and viscous Gilbert damping in ultrathin ferromagnets, Phys. Rev. B **73**, 144424 (2006).

[27] K. Zakeri, J. Lindner, I. Barsukov, R. Meckenstock, M. Farle, U. von Hörsten, H. Wende, W. Keune, J. Rocker, S. S. Kalarickal *et al.*, Spin dynamics in ferromagnets: Gilbert damping and two-magnon scattering, Phys. Rev. B **76**, 104416 (2007).

[28] H. Schultheiss, X. Janssens, M. van Kampen, F. Ciubotaru, S. J. Hermsdoerfer, B. Obry, A. Laraoui, A. A. Serga, L. Lagae, A. N. Slavin *et al.*, Direct Current Control of Three Magnon Scattering Processes in Spin-Valve Nanocontacts, Phys. Rev. Lett. **103**, 157202 (2009); https://www.ncbi.nlm.nih.gov/pubmed/19905663.

[29] H. Schultheiss, K. Vogt, and B. Hillebrands, Direct observation of nonlinear four-magnon scattering in spin-wave microconduits, Phys. Rev. B **86**, 054414 (2012).

[30] D. V. Slobodianiuk, G. A. Melkov, K. Schultheiss, H. Schultheiss, and R. V. Verba, Nonlinear ferromagnetic resonance in the presence of three-magnon scattering in magnetic nanostructures, IEEE Magn. Lett. **10**, 1 (2019).

[31] T. Hula, K. Schultheiss, A. Buzdakov, L. Körber, M. Bejarano, L. Flacke, L. Liensberger, M. Weiler, J. M. Shaw, H. T. Nembach *et al.*, Nonlinear losses in magnon transport due to four-magnon scattering, Appl. Phys. Lett. **117**, 042404 (2020).

[32] A. V. Chumak, A. A. Serga, and B. Hillebrands, Magnon transistor for all-magnon data processing, Nat. Commun. **5**, 4700 (2014); https://www.ncbi.nlm.nih.gov/pubmed/25144479.

[33] A. V. Chumak, V. I. Vasyuchka, A. A. Serga, and B. Hillebrands, Magnon spintronics, Nat. Phys. **11**, 453 (2015).

[34] V. F. Dmitriev and B. A. Kalinikos, Excitation of propagating magnetization waves by microstrip antennas, Sov. Phys. J. **31**, 875 (1988).

[35] T. Schneider, A. A. Serga, T. Neumann, B. Hillebrands, and M. P. Kostylev, Phase reciprocity of spin-wave excitation by a microstrip antenna, Phys. Rev. B **77**, 214411 (2008).

[36] F. Groß, M. Zelent, N. Träger, J. Förster, U. T. Sanli, R. Sauter, M. Decker, C. H. Back, M. Weigand, K. Keskinbora *et al.*, Building blocks for magnon optics: Emission and conversion of short spin waves, ACS Nano **14**, 17184 (2020); https://www.ncbi.nlm.nih.gov/pubmed/33253544.

[37] V. Vlaminck and M. Bailleul, Current-induced spin-wave doppler shift, Science **322**, 410 (2008).

[38] M. Madami, S. Bonetti, G. Consolo, S. Tacchi, G. Carlotti, G. Gubbiotti, F. B. Mancoff, M. A. Yar, and J. Åkerman, Direct observation of a propagating spin wave induced by spin-transfer torque, Nat. Nanotechnol. **6**, 635 (2011); https://www.ncbi.nlm.nih.gov/pubmed/21873993.

[39] Y. Au, E. Ahmad, O. Dmytriiev, M. Dvornik, T. Davison, and V. V. Kruglyak, Resonant microwave-to-spin-wave transducer, Appl. Phys. Lett. **100**, 182404 (2012).

[40] H. Yu, G. Duerr, R. Huber, M. Bahr, T. Schwarze, F. Brandl, and D. Grundler, Omnidirectional spin-wave nanograting coupler, Nat. Commun. **4**, 2702 (2013); https://www.ncbi.nlm.nih.gov/pubmed/24189978.

[41] H. Yu, O. d. A. Kelly, V. Cros, R. Bernard, P. Bortolotti, A. Anane, F. Brandl, F. Heimbach, and D. Grundler, Approaching soft X-ray wavelengths in nanomagnet-based microwave technology, Nat. Commun. **7**, 11255 (2016); https://www.ncbi.nlm.nih.gov/pmc/articles/PMC4831022/pdf/ncomms11255.pdf.

[42] F. Ciubotaru, T. Devolder, M. Manfrini, C. Adelmann, and I. P. Radu, All electrical propagating spin wave spectroscopy with broadband wavevector capability, Appl. Phys. Lett. **109**, 012403 (2016).

[43] S. Wintz, V. Tiberkevich, M. Weigand, J. Raabe, J. Lindner, A. Erbe, A. Slavin, and J. Fassbender, Magnetic vortex cores as tunable spin-wave emitters, Nat. Nanotechnol. **11**, 948 (2016); https://www.ncbi.nlm.nih.gov/pubmed/27428277.

[44] S. J. Hämäläinen, F. Brandl, K. J. A. Franke, D. Grundler, and S. van Dijken, Tunable Short-Wavelength Spin-Wave Emission and Confinement in Anisotropy-Modulated Multiferroic Heterostructures, Phys. Rev. Applied **8**, 014020 (2017).

[45] C. Liu, J. Chen, T. Liu, F. Heimbach, H. Yu, Y. Xiao, J. Hu, M. Liu, H. Chang, T. Stueckler *et al.*, Long-distance propagation of short-wavelength spin waves, Nat. Commun. **9**, 738 (2018); https://www.ncbi.nlm.nih.gov/pubmed/29467416.

[46] H. Qin, G. J. Both, S. J. Hamalainen, L. Yao, and S. van Dijken, Low-loss YIG-based magnonic crystals with large tunable bandgaps, Nat. Commun. **9**, 5445 (2018); https://www.ncbi.nlm.nih.gov/pubmed/30575742.

[47] G. Dieterle, J. Forster, H. Stoll, A. S. Semisalova, S. Finizio, A. Gangwar, M. Weigand, M. Noske, M. Fahnle, I. Bykova *et al.*, Coherent Excitation of Heterosymmetric Spin Waves with Ultrashort Wavelengths, Phys. Rev. Lett. **122**, 117202 (2019); https://www.ncbi.nlm.nih.gov/pubmed/30951356.

[48] J. Förster, J. Gäfe, J. Bailey, S. Finizio, N. Träger, F. Groß, S. Mayr, H. Stoll, C. Dubs, O. Surzhenko *et al.*, Direct observation of coherent magnons with suboptical wavelengths in a single-crystalline ferrimagnetic insulator, Phys. Rev. B **100**, 214416 (2019).

[49] P. Che, K. Baumgaertl, A. Kukol'ova, C. Dubs, and D. Grundler, Efficient wavelength conversion of exchange magnons below 100 nm by magnetic coplanar waveguides, Nat. Commun. **11**, 1445 (2020); https://www.ncbi.nlm.nih.gov/pubmed/32193377.

[50] C. Koerner, R. Dreyer, M. Wagener, N. Liebing, H. G. Bauer, and G. Woltersdorf, Frequency multiplication by collective nanoscale spin-wave dynamics, Science **375**, 1165 (2022).

[51] F. Groß, M. Zelent, A. Gangwar, S. Mamica, P. Gruszecki, M. Werner, G. Schütz, M. Weigand, E. J. Goering, C. H. Back,

et al., Phase resolved observation of spin wave modes in antidot lattices, Appl. Phys. Lett. **118**, 232403 (2021).

[52] A. Vansteenkiste, J. Leliaert, M. Dvornik, M. Helsen, F. Garcia-Sanchez, and B. Van Waeyenberge, The design and verification of MuMax3, AIP Adv. **4**, 107133 (2014).

[53] Felix Groß, N. Träger, J. Förster, M. Weigand, G. Schütz, and J. Gräfe, Nanoscale detection of spin wave deflection angles in permalloy, Appl. Phys. Lett. **114**, 012406 (2019).

[54] N. Träger, P. Gruszecki, F. Lisiecki, F. Groß, J. Förster, M. Weigand, H. Gowiski, P. Kuwik, J. Dubowik, M. Krawczyk *et al.*, Demonstration of *k*-vector selective microscopy for nanoscale mapping of higher order spin wave modes, Nanoscale **12**, 17238 (2020); https://www.ncbi.nlm.nih.gov/pubmed/32558843.

[55] D. Nolle, M. Weigand, P. Audehm, E. Goering, U. Wiesemann, C. Wolter, E. Nolle, and G. Schütz, Note: unique characterization possibilities in the ultra high vacuum scanning transmission x-ray microscope (UHV-STXM) "MAXYMUS" using a rotatable permanent magnetic field up to 0.22 T, Rev. Sci. Instrum. **83**, 046112 (2012); https://www.ncbi.nlm.nih.gov/pubmed/22559598.

[56] G. Schütz, W. Wagner, W. Wilhelm, P. Kienle, R. Zeller, R. Frahm, and G. Materlik, Absorption of Circularly Polarized X Rays in Iron, Phys. Rev. Lett. **58**, 737 (1987); https://www.ncbi.nlm.nih.gov/pubmed/10035022.

[57] F. Groß, N. Träger, and J. Gräfe, MIEP A time-resolved X-ray image evaluation program, SoftwareX **15**, 100705 (2021).

[58] J. Gräfe, M. Weigand, B. Van Waeyenberge, A. Gangwar, F. Groß, F. Lisiecki, J. Rychly, H. Stoll, N. Träger, J. Förster, F. Stobiecki, J. Dubowik, J. Klos, M. Krawczyk, C. H. Back, E. J. Goering, and G. Schütz, Visualizing nanoscale spin waves using MAXYMUS, Proc. SPIE, **11090**, 1109025 (2019).

[59] F. Lisiecki, J. Rychy, P. Kuwik, H. Gowiski, J. W. Kos, F. Groß, I. Bykova, M. Weigand, M. Zelent, E. J. Goering *et al.*, Reprogrammability and Scalability of Magnonic Fibonacci Quasicrystals, Phys. Rev. Applied **11**, 054003 (2019).

[60] F. Lisiecki, J. Rychy, P. Kuwik, H. Gowiski, J. W. Kos, F. Groß, N. Träger, I. Bykova, M. Weigand, M. Zelent *et al.*, Magnons in a Quasicrystal: Propagation, Extinction, and Localization of Spin Waves in Fibonacci Structures, Phys. Rev. Applied **11**, 054061 (2019).

[61] Nick Träger, F. Groß, J. Förster, K. Baumgaertl, H. Stoll, M. Weigand, G. Schütz, D. Grundler, and J. Gräfe, Single shot acquisition of spatially resolved spin wave dispersion relations using X-ray microscopy, Sci. Rep. **10**, 18146 (2020); https://www.ncbi.nlm.nih.gov/pubmed/33097751.

[62] N. Träger, P. Gruszecki, F. Lisiecki, F. Groß, J. Förster, M. Weigand, H. Gowiski, P. Kuwik, J. Dubowik, G. Schütz *et al.*, Real-Space Observation of Magnon Interaction with Driven Space-Time Crystals, Phys. Rev. Lett. **126**, 057201 (2021).

[63] See Supplemental Material at http://link.aps.org/supplemental/10.1103/PhysRevB.106.014426 for experimental examples of frequency multiplication at base frequencies of 1.41 GHz and 1.87 GHz.

[64] A. G. Gurevich and G. A. Melkov, *Magnetization Oscillations and Waves* (CRC Press, London, 1996).